Crucial Role of the Adhesion Layer on the Plasmonic Fluorescence Enhancement

Heykel Aouani,[†] Jérôme Wenger,[†,*] Davy Gérard,[†,||] Hervé Rigneault,[†] Eloïse Devaux,[‡] Thomas W. Ebbesen,[‡] Farhad Mahdavi,[§] Tingjun Xu,[§] and Steve Blair[§]

[†]Institut Fresnel, Aix-Marseille Université, CNRS, Ecole Centrale Marseille, Campus de St. Jérôme, 13397 Marseille, France, [‡]Institut de Science et d'Ingénierie Supramoléculaires, Université Louis Pasteur, CNRS, 8 allée G. Monge, 67000 Strasbourg, France, and [§]Electrical and Computer Engineering Department, University of Utah, 50 South Central Campus Drive, Rm. 3280, Salt Lake City, Utah 84112. [||]Current address: LNIO, Institut Charles Delaunay, Université de Technologie de Troyes, France.

ABSTRACT A nanoscale layer of chromium or titanium is commonly used in plasmonic nanoantennas to firmly adhere a gold film to a glass substrate, yet the influence of this layer on the antenna performance is often ignored. As a result, the need for the use of potentially better materials is not widely recognized. Using a single aperture milled in a gold film with 120 nm diameter as a nanobench for these investigations, we present the first experimental report of the strong dependence of the plasmonic enhancement of single-molecule fluorescence on the nature of the adhesion layer. By combining fluorescence correlation spectroscopy and fluorescence lifetime measurements, we show that this structure is very sensitive to the properties of the adhesion layer, and we detail the respective contributions of excitation and emission gains to the observed enhanced fluorescence. Any increase in the absorption losses due to the adhesion layer permittivity or thickness is shown to lower the gains in both excitation and emission, which we relate to a damping of the energy coupling at the nanoaperture. With this nanobench, we demonstrate the largest enhancement factor reported to date (25×) by using a TiO_2 adhesion layer. The experimental data are supported by numerical simulations and argue for a careful consideration of the adhesion layer while designing nanoantennas for high-efficiency single-molecule analysis.

KEYWORDS: plasmonics · nanoantennas · metal nanoapertures · fluorescence enhancement · fluorescence correlation spectroscopy · nanofabrication

Plasmonic nanoantennas have gained great interest in recent years for applications in nanophotonics,[1−3] enhanced light emission,[4−6] and molecular sensing.[7−9] Comprehensive theoretical and experimental studies have been performed to characterize antennas made of coupled metallic nanoparticles in a large variety of shapes and geometries.[10−14] While gold is widely used to fabricate these plasmonic components, a supplementary adhesion layer (generally made of chromium or titanium) is needed to ensure firm contact between the gold film and the substrate. However, detailed understanding is still lacking regarding the role of this adhesion layer on the plasmonic resonances. It has been experimentally observed that a thin intermediate chromium or titanium layer shifts and broadens the surface plasmon resonance in the case of a flat interface[15−17] or of gold nanodiscs.[18] The magnitude of the resonance has also been found to decrease when the thickness of the adhesion layer increases. The case of resonant bowtie nanoantennas has been recently numerically modeled.[19] It was found that the influence of adhesion layers lies on the complex dielectric constant of the material. For dielectric adhesion layers, the influence of the refractive index causes the plasmonic resonance to red shift and decrease in strength. It was also found to modify the field localization within the nanoantenna by pushing the high-intensity region to the top of the structure when illuminated from below. For metal adhesion layers, the intrinsic absorption quenches the resonance at the bottom of the structure, while causing the resonances within the gap to red shift from top to bottom. Adhesion layer engineering can thus be used to optimize the near-field localization inside the antenna.

To bridge the gap between numerical modeling and experimental observations of the influence of adhesion layers in plasmonics, we take advantage of the techniques recently developed by our team to characterize the fluorescence emission within single nanometric apertures milled in a gold film (Figure 1). The nanoaperture structure offers a reliable test bench for such studies,[20,21] as it can be reproducibly fabricated with robust techniques, and it has been proven to be a sensitive platform to study enhanced fluorescence emission of single molecules.[22,23] To investigate the influence of the adhesion layer, we focus here on 120 nm diameter apertures milled in a 200 nm thick gold film with different

*Address correspondence to jerome.wenger@Fresnel.fr.

Received for review May 6, 2009 and accepted June 06, 2009.

Published online June 11, 2009.
10.1021/nn900460t CCC: $40.75

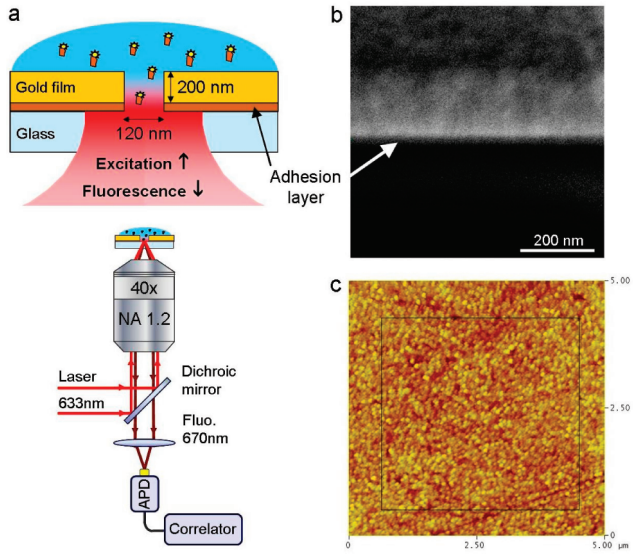

Figure 1. (a) Schematics of the experimental configuration. (b) Scanning electron microscope view along the side of the sample. The sample has been cut with FIB and is strongly tilted to show the stack of layers. The dark region indicated by the white arrow corresponds to the adhesion layer. (c) Atomic force microscopy view of the upper surface of the gold film. The rms roughness in the area indicated by the square is measured to 1.5 nm.

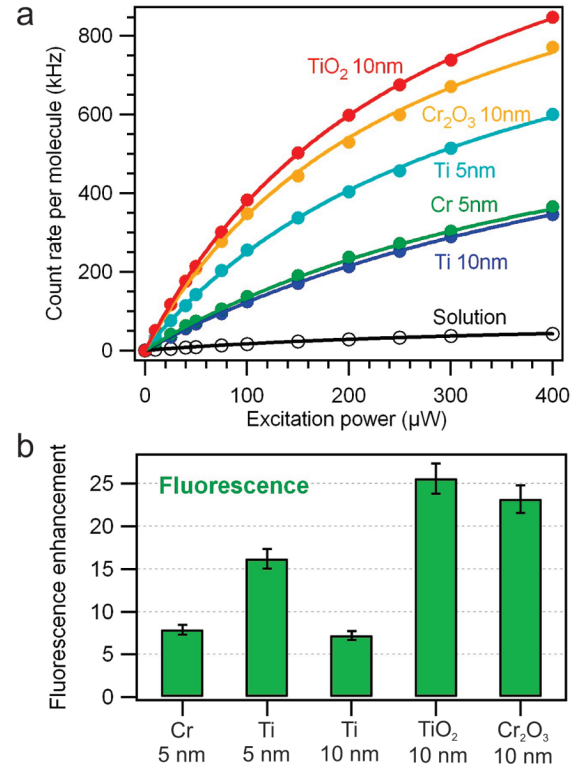

Figure 2. (a) Count rate per molecule *versus* the excitation power within a single 120 nm aperture with different adhesion layers. Markers are experimental data, solid lines are numerical fits (see text). Fitting parameters are summarized in Table 1. (b) Fluorescence rate enhancement in the regime below saturation deduced from the numerical fits in (a).

adhesion layers: 5 nm of chromium or titanium, 10 nm of titanium, and 10 nm of titanium oxide (TiO_2) or chromium oxide (Cr_2O_3). Other configurations were also tested, yet to maintain the readability of our results, we select only these five cases as the most insightful. The aperture diameter is chosen to yield the maximum fluorescence enhancement at 633 nm excitation, as already reported.[22,23] For each sample, the fluorescence emission of Alexa Fluor 647 molecules diffusing within the structure is characterized according to the procedure developed in ref 23. This method relies on a combination of fluorescence correlation spectroscopy (FCS) with fluorescence time-correlated lifetime measurements. It specifically allows one to detail the influence of the nanostructure on the molecular emission and quantifies the respective weights of excitation and emission contributions to the observed enhanced fluorescence.

RESULTS

We start by performing a set of FCS measurements while increasing the excitation power from 10 to 400 μW (the upper limit was set to avoid damaging the sample and photobleaching the dyes). Each FCS correlation function is analyzed to reliably measure the fluorescence count rate per molecule, CRM (see Methods section). For each excitation power, special care is taken to characterize the level of background noise and the dark state amplitude. Results are summarized in Figure 2a, in the case of an open solution and in the case of 120 nm apertures with different adhesion layers. It is apparent from this raw data that the nature of the adhesion layer has a dramatic impact on the fluorescence emission. To make this effect appear even clearer, we model this data with the expression of the fluorescence rate given by $CRM = A(I_e)/(1 + I_e/I_s)$, where I_e is the excitation intensity, I_s the saturation intensity, and A is a constant proportional to the molecular absorption cross section, quantum yield, and setup collection efficiency.[24] The fitting parameters are summarized in Table 1 and are used hereafter to compare the different adhesion layers.

Figure 2b displays the fluorescence rate enhancement for the different adhesion layers found in the regime below saturation. This factor is defined as the ratio of the detected fluorescence rate per molecule in

TABLE 1. Refractive Index (*n*) and Extinction Coefficient (*k*) of the Different Materials Used Here at 633 nm Wavelength, Taken from Ref 19[a]

material	Cr	Ti	Ti	TiO_2	Cr_2O_3	sol
thickness (nm)	5	5	10	10	10	
n	3.54	2.15	2.15	1.97	2.45	
k	4.36	2.92	2.92	0	0.54	
A (kHz/μW)	1.6	3.2	1.4	5.1	4.6	0.2
I_s (μW)	480	320	600	280	270	435
τ (ns)	0.41	0.40	0.36	0.40	0.40	0.88

[a]The table also presents the fitting parameters A, I_s for the experimental data in Figure 2a and the fluorescence lifetime τ in Figure 3a.

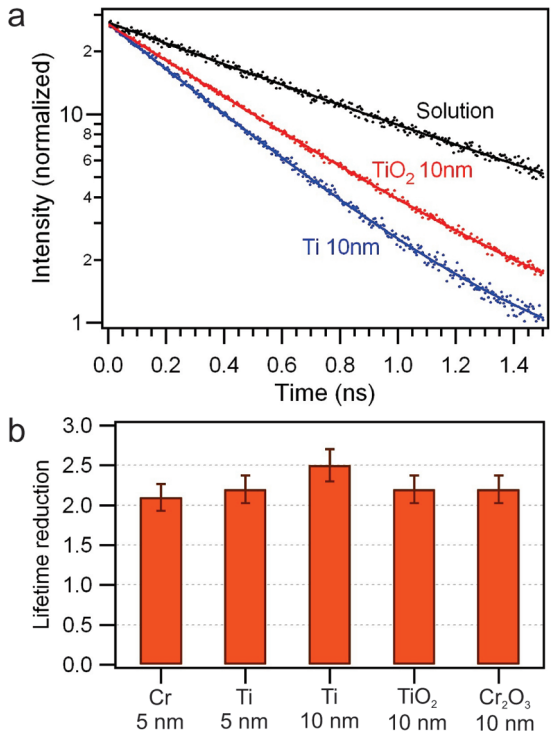

Figure 3. (a) Normalized fluorescence decay traces measured in open solution (black dots) and in single 120 nm apertures with 10 nm Ti or TiO_2 adhesion layer. Dots are experimental data, lines are numerical fits. The other adhesion layers used in this study resulted in traces almost identical to the one of the TiO_2 case; they are therefore not represented here to maintain clarity. (b) Fluorescence lifetime reduction as compared to molecules in open solution for the different adhesion layers.

the aperture with respect to the CRM in open solution taken at the limit of low excitation $I_e \rightarrow 0$. Practically, it corresponds to the ratio of the *A* parameters derived from the interpolation of the data curves in Figure 2a, which are given in Table 1.

A striking 25-fold fluorescence enhancement is found for a 10 nm TiO_2 layer and is the highest gain reported to date for Alexa Fluor 647 molecules in a nanoaperture. This value has to be compared to the 7.2 enhancement found instead for a 10 nm Ti layer. Although the same preparation procedures and experimental setup are used, the net difference between the fluorescence signal per emitter can be as large as 3.5-fold. At least seven different apertures are tested for each adhesion layer, with variation in fluorescence count rate between 6 and 8%, which takes into account effects such as dispersion in aperture diameter. The error bars displayed in Figure 2b indicate the standard deviations of our measurements.

Metallic adhesion layers, such as Cr and Ti, are shown to yield lower overall fluorescence enhancements and greater saturation intensities than dielectric layers. This can be understood as a stronger damping of the plasmonic resonance due to an increased absorption in the adhesion layer and corroborates the conclusions drawn in ref 19. The negative effect of losses is confirmed by the lower enhancement found for chromium compared to that for titanium at a fixed thickness (chromium's absorption is about three times that of titanium at 633 nm; see Table 1) and by the fact that the fluorescence enhancement increases when the adhesion layer thickness decreases. Last, the damping effect of absorption is also exhibited for dielectrics, with a higher enhancement for titanium oxide (which shows negligible absorption in the visible range) than for chromium oxide (which has some residual absorption at 633 nm). Almost every experimental study of plasmonic nanoantennas skips the issue of the adhesion layer choice and design, while we clearly show here that it has a dramatic influence.

To complete the FCS measurements and fully characterize the fluorescence enhancement phenomenon, we conduct time-correlated single photon counting (TCSPC) experiments to monitor the fluorescence lifetime alteration inside the nanoapertures. These experiments are performed for the same nanoaperture sample and the Alexa Fluor 647 solution. Figure 3a shows the fluorescence decay curves for molecules in open solution and in single 120 nm apertures with 10 nm Ti or TiO_2 adhesion layer. The other adhesion layers used in this study resulted in traces nearly identical to the one of the TiO_2 case and are not represented to ease viewing the graphs. The fluorescence decay rate is measured by fitting the data using a single exponential decay model convolved by the calibrated instrument response function.[23] This yields the fluorescence lifetime reduction normalized to the open solution case displayed in Figure 3b. Interestingly, this factor appears almost independent of the adhesion layer, showing that the near-field molecular decay routes in the nanoaperture are dominated by the gold structure, not by the adhesion layer. However, the coupling of the fluorescence radiation to the far-field is affected by the adhesion layer, as shown on Figure 2 and discussed hereafter.

DISCUSSION

Different effects can lead to an enhancement of the fluorescence signal of a single molecule: (i) local increase in the excitation intensity, (ii) increases in the emitter's radiative rate and quantum efficiency, and (iii) modification of the emitter's radiation pattern, giving a higher emission directionality toward the detectors. Determining the relative influence of these effects is a delicate task, which can be addressed by combining FCS with fluorescence lifetime measurements. As discussed in the Methods section, the gain in emission, η_{em}, is derived from the value of the fluorescence enhancement in the saturation regime, which we obtain from the asymptotic interpolation of the data points in Figure 2a at the limit where $I_e \rightarrow \infty$. The gain in excitation inten-

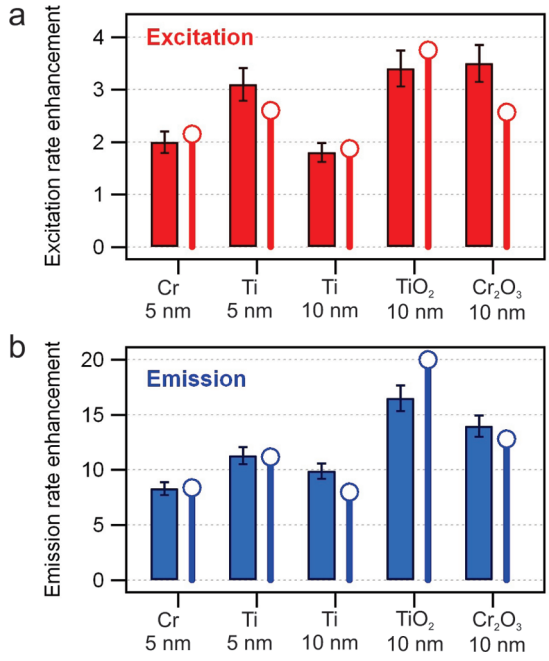

Figure 4. Contributions of excitation (a) and emission gains (b) to the fluorescence enhancement found for different adhesion layers. Bars are experimental data, empty circles are for numerical computations.

sity, η_{exc}, equals the fluorescence enhancement in the low excitation regime divided by the ratio of the emission gain by the total decay rate alteration: $\eta_{exc} = \eta_F/(\eta_{em}/\eta_{tot})$.

This procedure yields the experimental estimates of the excitation and emission gains for the different adhesion layers displayed in Figure 4. The gain in excitation intensity can be understood as a better coupling of energy inside the nanostructure, while the gain in emission has to be related to a better outcoupling of the energy stored in the dipole's near-field to the detected far-field radiation. Due to the small Stokes shift between the excitation and emission wavelengths of Alexa Fluor 647, the reciprocity theorem holds and, consequently, both excitation and emission phenomena influence the overall gain in fluorescence and show strong variations with the nature of the adhesion layer used. Absorption in metallic adhesion layers yields lower gains than dielectric layers for both excitation and emission. These data confirm that any increase in absorption losses due to the material's properties or an increased thickness results in a damping of the near- to far-field coupling at the nanoaperture.

To supplement this experimental evidence, we conduct a numerical analysis based on the finite element method (see Methods section). This method allows one to separately compute the enhancements in excitation intensity and emission rate, which both contribute to the overall gain in the fluorescence signal. The increase of the excitation intensity inside the aperture is computed from the average intensity measured with and without the nanostructure at a plane located 20 nm inside the aperture. For the emission calculations, we compute the radiative emission through the glass side by integrating the *z*-component of Poynting's vector across a plane located 20 nm below the metal surface for single dipoles located in different positions and orientations inside the aperture (see Methods section). Results of numerical simulations for excitation and emission are displayed in Figure 4 for the different adhesion layers (empty markers). They are remarkably consistent with the experimental data and confirm the crucial influence of the adhesion layer on both excitation and emission gains in the nanostructure. Interestingly, this method allows one to predict the maximum fluorescence enhancement for gold only with no adhesion layer. We obtain an optimum fluorescence enhancement of 28 for Alexa Fluor 647 molecules, which is about 10% higher than with the 10 nm TiO_2 layer. This confirms that titanium oxide is the material of choice for practical plasmonic enhancement applications.

CONCLUSIONS

We experimentally and numerically study the influence of the adhesion layer commonly used to ensure firm contact between a gold film and underlying glass substrate in plasmonic nanoantennas. A single aperture milled in the metal film with 120 nm diameter forms a reliable structure to investigate the effects of the adhesion layer on the fluorescence enhancement of single molecules. Although the same preparation procedures and experimental setup are used, we show that the nature of the adhesion layer (permittivity and thickness) has a dramatic impact on the fluorescence signal per molecule with a difference up to a factor of 4. By combining FCS and fluorescence lifetime measurements, we detail the respective contributions of excitation and emission gains to the observed enhanced fluorescence. Any increase in the absorption losses due to the adhesion layer material's properties or increased thickness is shown to yield lower enhancements, which we relate to a damping of the near- to far-field coupling at the nanoaperture. The experimental data are sustained by numerical simulations using finite element method. To our knowledge, this is the first experimental report of the strong dependence of the fluorescence gain on the nature of the adhesion layer. Clearly, one has to consider the role of the adhesion layer while designing nanoantennas for high-efficiency single-molecule analysis based on either fluorescence or Raman scattering, 10 nm of titanium oxide being the optimal choice based upon our study.

METHODS

Nanoaperture Fabrication. All metal and dielectric films are deposited using reactive DC magnetron sputtering in the same chamber. The gold film thickness of 200 nm was chosen to be optically opaque and isolate the molecules diffusing in the aperture from the pool of molecules lying above the structure. Adhesion between the gold film and the 150 μm thick glass substrate is ensured by a layer of 5 nm of chromium or titanium, 10 nm of titanium, or 10 nm of titanium oxide (TiO_2) or chromium oxide (Cr_2O_3). The oxides' adhesion layers are deposited using the same metal targets, but under partial oxygen pressure. Thickness control is maintained by a cluster of piezoelectric monitors. We relied on calibration of the deposition process using quartz crystal monitors and test samples. Therefore, we estimate no more than 20% error in the adhesion layer thickness. Similar adhesion properties were found for these different layers. Last, circular apertures of 120 nm diameter are milled by focused ion beam (FEI Strata DB235). We checked that the metal film roughness remained similar for all adhesion layers used. Figure 1c presents a typical AFM image of the upper gold surface, where the roughness was measured to 1.5 nm.

Fluorescence Count Rate per Molecule Calibration. In order to get an accurate understanding of the fluorescence emission in the nanostructure and investigate the influence of the adhesion layer, it is crucial to quantify the fluorescence count rate *per molecule CRM*, which requires the knowledge of the actual number of emitters, N, contributing to the global fluorescence signal. This issue is addressed *via* fluorescence correlation spectroscopy (FCS).[24] In FCS, the temporal fluctuations, $F(t)$, of the fluorescence signal are recorded, and the temporal correlation of this signal is computed $g^{(2)}(\tau) = \langle F(t) \times F(t+\tau)\rangle/\langle F(t)\rangle^2$, where τ is the delay (lag) time, and $\langle\ \rangle$ is for time averaging. Analysis of the correlation function provides a measure for the number of molecules, N, needed to compute the count rate per molecule CRM $= \langle F\rangle/N$.[22,23] We point out that, as a consequence of the stochastic nature of the FCS technique, all the presented fluorescence data are spatially averaged over all the possible molecule orientations and positions inside the detection volume.

Excitation and Emission Gains Characterization. To unravel the origins of the fluorescence enhancement near a photonic structure, we have developed a specific experimental procedure which has already been applied to the case of fluorescence alteration by gold nanometric apertures.[23] This procedure can be summarized as follows: the fluorescence rates per molecule CRM are measured for increasing excitation powers in open solution and in the case of a nanoaperture. The resulting data points are fitted according to the model CRM $= A(I_e)/(1 + I_e/I_s)$, where I_e is the excitation intensity, I_s the saturation intensity, and A is a constant proportional to the molecular absorption cross section, quantum yield, and setup collection efficiency.[24] We deduce from the fits the fluorescence enhancements at the two extreme cases below saturation $I_e \ll I_s$ and at saturation $I_e \gg I_s$. In the saturation regime, the fluorescence rate enhancement is determined only by the gain in emission, η_{em}. In the low excitation regime, $I_e \ll I_s$, the fluorescence enhancement, η_F, is proportional to the gains in emission, η_{em}, and local excitation intensity, η_{exc}, and inversely proportional to the gain in total fluorescence decay rate, η_{tot}: $\eta_F = \eta_{em}\eta_{exc}/\eta_{tot}$. Using supplementary fluorescence lifetime measurements to determine the alteration in the total fluorescence decay rate, η_{tot}, it is therefore possible to extract the gain in local excitation intensity from the fluorescence enhancement in the low excitation regime. This unambiguously separates the excitation and emission contributions to the total fluorescence enhancement and is used here to investigate the influence of the adhesion layer on the fluorescence enhancement in single nanoapertures.

Experimental Setup. A comprehensive description of our experimental setup has been presented before.[23] Briefly, it is based on a confocal inverted microscope with a NA = 1.2 water-immersion objective, allowing single aperture studies (Figure 1a). For all experiments reported here, we use an aqueous solution of Alexa Fluor 647 fluorescent molecules (A647, Invitrogen, Carlsbad, CA) deposited on top of the sample with micromolar concentration. These molecules are constantly diffusing in and out of the aperture, thereby limiting photobleaching. For FCS measurements, the excitation source is a CW He−Ne laser operating at 633 nm. For lifetime measurements, the excitation source is a picosecond laser diode operating at 636 nm (PicoQuant LDH-P-635). A single-mode optical fiber ensures a perfect spatial overlap between the pulsed laser diode and the CW laser. Accurate positioning of the nanoaperture at the laser focus spot is obtained with a multiaxis piezoelectric stage. Single photon detection is performed by avalanche photodiodes with 670 ± 20 nm fluorescence band-pass filters. For FCS, the fluorescence intensity temporal fluctuations are analyzed with a ALV6000 hardware correlator. Each individual FCS measurement is obtained by averaging 10 runs of 10 s duration. For fluorescence lifetime measurements, the photodiode output is coupled to a fast time-correlated single photon counting module (PicoQuant PicoHarp 300).

Numerical Simulations. Numerical analysis is based on the finite element method using COMSOL Multiphysics version 3.3.[25] The model considers a computational space of 1.0 × 1.0 × 1.1 μm^3, with radiation boundary conditions on all faces. A glass substrate is put underneath a 200 nm thick layer of gold plus a 5 or 10 nm adhesion layer, the upper region being water. Gold dielectric properties are incorporated as measured by spectroscopic ellipsometry.[19,25] A single 120 nm aperture is placed in the center of the metal. To estimate the increase of the excitation intensity inside the aperture, a plane wave at 633 nm is launched incoming from the glass side. Electromagnetic intensity is measured and averaged over the plane 20 nm inside the aperture. This result is then normalized by the integrated intensity with no metal layer. For the emission calculations, a 1 nm dipole is positioned at various locations inside the aperture. Eleven horizontal planes 20 nm apart are considered in the aperture, the very first and very last planes being 5 nm inside the structure. In each horizontal plane, 37 dipole positions are taken. At each point, a dipole emitting at 670 nm is aligned along X, Y, and Z directions. The radiative emission through the glass side is estimated by integrating the z-component of Poynting's vector across a plane located 20 nm below the metal surface. This averaged power is then scaled by a fixed normalization factor to fit the experimental emission gain for the chromium adhesion layer.

Acknowledgment. The authors acknowledge stimulating discussions with N. Bonod and E. Popov. This work has been funded by the French Agence Nationale de la Recherche under contract ANR-07-NANO-006-03 "ANTARES" and the U.S. National Science Foundation Grants ECS-0622225 and ECS-0637121.

REFERENCES AND NOTES

1. Barnes, W. L.; Dereux, A.; Ebbesen, T. W. Surface Plasmon Subwavelength Optics. *Nature* **2003**, *424*, 824–830.
2. Novotny, L. Effective Wavelength Scaling for Optical Antennas. *Phys. Rev. Lett.* **2007**, *98*, 266802.
3. Sundaramurthy, A.; Schuck, P. J.; Conley, N. R.; Fromm, D. P.; Kino, G. S.; Moerner, W. E. Toward Nanometer-Scale Optical Photolithography: Utilizing the Near-Field of Bowtie Optical Nanoantennas. *Nano Lett.* **2006**, *6*, 355–360.
4. Muhlschlegel, P.; Eisler, H. J.; Martin, O. J. F.; Hecht, B.; Pohl, D. W. Resonant Optical Antennas. *Science* **2005**, *308*, 1607–1609.
5. Yu, N. F.; Cubukcu, E.; Diehl, L.; Bour, D.; Corzine, S.; Zhu, J. T.; Hofler, G.; Crozier, K. B.; Capasso, F. Bowtie Plasmonic Quantum Cascade Laser Antenna. *Opt. Express* **2007**, *15*, 13272–13281.
6. Kim, S.; Jin, J.; Kim, Y.-J.; Park, I.-Y.; Kim, Y.; Kim, S.-W. High-Harmonic Generation by Resonant Plasmon Field Enhancement. *Nature* **2008**, *453*, 757–760.
7. Muskens, O. L.; Giannini, V.; Sanchez-Gil, J. A.; Rivast, J. G. Strong Enhancement of the Radiative Decay Rate of Emitters by Single Plasmonic Nanoantennas. *Nano Lett.* **2007**, *7*, 2871–2875.

8. Bakker, R. M.; Yuan, H. K.; Liu, Z. T.; Drachev, V. P.; Kildishev, A. V.; Shalaev, V. M.; Pedersen, R. H.; Gresillon, S.; Boltasseva, A. Enhanced Localized Fluorescence in Plasmonic Nanoantennae. *Appl. Phys. Lett.* **2008**, *92*, 43101–43104.
9. Fu, Y.; Lakowicz, J. R. Modification of Single Molecule Fluorescence near Metallic Nanostructures. *Laser Photon. Rev.* **2009**, *3*, 221232.
10. Genov, D. A.; Sarychev, A. K.; Shalaev, V. M.; Wei, A. Resonant Field Enhancements from Metal Nanoparticle Arrays. *Nano Lett.* **2004**, *4*, 153–158.
11. Sundaramurthy, A.; Crozier, K. B.; Kino, G. S.; Fromm, D. P.; Schuck, P. J.; Moerner, W. E. Field Enhancement and Gap-Dependent Resonance in a System of Two Opposing Tip-to-Tip Au Nano- Triangles. *Phys. Rev. B* **2005**, *72*, 165409.
12. Sondergaard, T.; Bozhevolnyi, S. Slow-Plasmon Resonant Nanostructures: Scattering and Field Enhancements. *Phys. Rev. B* **2007**, *75*, 073402.
13. Rogobete, L.; Kaminski, F.; Agio, M.; Sandoghdar, V. Design of Plasmonic Nanoantennae for Enhancing Spontaneous Emission. *Opt. Lett.* **2007**, *32*, 1623–1625.
14. Fischer, H.; Martin, O. J. F. Engineering the Optical Response of Plasmonic Nanoantennas. *Opt. Express* **2008**, *16*, 9144–9154.
15. Neff, H.; Zong, W.; Lima, A. M. N.; Borre, M.; Holzhuter, G. Optical Properties and Instrumental Performance of Thin Gold Films near the Surface Plasmon Resonance. *Thin Solid Films* **2006**, *496*, 688–697.
16. Sexton, B. A.; Feltis, B. N.; Davis, T. J. Characterisation of Gold Surface Plasmon Resonance Sensor Substrates. *Sens. Actuators, A* **2008**, *141*, 471–475.
17. Barchiesi, D.; Macias, D.; Belmar-Letellier, L.; van Labeke, D.; Lamy de la Chapelle, M.; Toury, T.; Kremer, E.; Moreau, L.; Grosges, T. Plasmonics: Influence of the Intermediate (or Stick) Layer on the Efficiency of Sensors. *Appl. Phys. B* **2008**, *93*, 177181.
18. Kim, J.; Cho, K.; Lee, K.-S. Effect of Adhesion Layer on the Optical Scattering Properties of Plasmonic Au Nanodisc. *J. Korean Inst. Met. Mater.* **2008**, *46*, 464–470.
19. Jiao, X.; Goeckeritz, J.; Blair, S.; Oldham, M. Localization of Near-Field Resonances in Bowtie Antennae: Influence of Adhesion Layers. *Plasmonics* **2009**, *4*, 37–50.
20. Genet, C.; Ebbesen, T. W. Light in Tiny Holes. *Nature* **2007**, *445*, 39–46.
21. Lenne, P. F.; Rigneault, H.; Marguet, D.; Wenger, J. Fluorescence Fluctuations Analysis in Nanoapertures: Physical Concepts and Biological Applications. *Histochem. Cell Biol.* **2008**, *130*, 795805.
22. Gérard, D.; Wenger, J.; Bonod, N.; Popov, E.; Rigneault, H.; Mahdavi, F.; Blair, S.; Dintinger, J.; Ebbesen, T. W. Nanoaperture-Enhanced Fluorescence: Towards Higher Detection Rates with Plasmonic Metals. *Phys. Rev. B* **2008**, *77*, 045413.
23. Wenger, J.; Gérard, D.; Bonod, N.; Popov, E.; Rigneault, H.; Dintinger, J.; Mahboub, O.; Ebbesen, T. W. Emission and Excitation Contributions to Enhanced Single Molecule Fluorescence by Gold Nanometric Apertures. *Opt. Express* **2008**, *16*, 3008–3020.
24. Zander, C., Enderlein, J., Keller, R. A., Eds. *Single-Molecule Detection in Solution: Methods and Applications*; Wiley-VCH: Berlin/New York, 2002.
25. Mahdavi, F.; Liu, Y.; Blair, S. Modeling Fluorescence Enhancement from Metallic Nanocavities. *Plasmonics* **2007**, *2*, 129–142.